Performance Analysis of Aircraft-to-Ground Communication Networks in Urban Air Mobility (UAM)

Tengchan Zeng, Omid Semiari, Walid Saad, and Mehdi Bennis

***Abstract*—To meet the growing mobility needs in intra-city transportation, urban air mobility (UAM) has been proposed in which vertical takeoff and landing (VTOL) aircraft are used to provide on-demand service. In UAM, an aircraft can operate in the corridors, i.e., the designated airspace, that link the aerodromes, thus avoiding the use of complex routing strategies such as those of modern-day helicopters. For safety, a UAM aircraft will use air-to-ground communications to report flight plan, off-nominal events, and real-time movements to ground base stations (GBSs). A reliable communication network between GBSs and aircraft enables UAM to adequately utilize the airspace and create a fast, efficient, and safe transportation system. In this paper, to characterize the wireless connectivity performance in UAM, a stochastic geometry-based spatial model is developed. In particular, the distribution of GBSs is modeled as a Poisson point process (PPP), and the aircraft are distributed according to a combination of PPP, Poisson cluster process (PCP), and Poisson line process (PLP). For this setup, assuming that any given aircraft communicates with the closest GBS, the distribution of distance between an arbitrarily selected GBS and its associated aircraft and the Laplace transform of the interference experienced by the GBS are derived. Using these results, the signal-to-interference ratio (SIR)-based connectivity probability is determined to capture the connectivity performance of the aircraft-to-ground communication network in UAM. Simulation results validate the theoretical derivations for the UAM wireless connectivity and provide useful UAM design guidelines by showing the connectivity performance under different parameter settings.**

I. Introduction

According to the world urbanization prospects released by the United Nations, by 2030, more than 60% of the world's population will live in urban areas and this percentage will jump to 70% by 2050 [1]. Given this growth, mobility demands will push the ground transportation system to its limits, leading to a long commute for the public and significant economic costs for the society. In order to meet future mobility needs, the novel concept of urban air mobility (UAM) was proposed [2]. Different from traditional ground traffic, UAM will introduce a fully automated vertical takeoff and landing (VTOL) aircraft to integrate the third dimension, i.e., airspace above cities, into the urban transportation system. Recent technology advances on distributed electric propulsion, electrical energy storage, lightweight airframe structures, and electric VTOL will make UAM a reality [2].

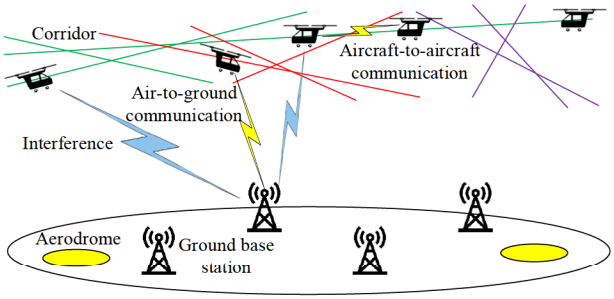

Fig. 1. Illustration of the urban air mobility (UAM) model.

As shown in Fig. 1, a UAM system is composed of VTOL aircraft, aerodromes, corridors, and ground base stations (GBSs). In particular, aerodromes are designed to support the arrival and departure operation of the aircraft. Moreover, the corridors linking different aerodromes constitute the airspace designated for UAM operation. Different from the complex routing strategy used by current helicopter applications, the idea of corridors can dramatically reduce the operational complexity [2]. Also, due to the common mobility patterns shared by the public, corridors are usually concentrated around specific locations, such as residential, shopping, and business areas. In addition, GBSs in UAM will function as service providers that constantly communicate with the aircraft and deliver necessary information (e.g., weather and terrain), approve the flight plan submitted by the aircraft, and monitor the movements of aircraft.

Each UAM operation has two major phases: *planning* and *en-route*. In the planning phase, once the aircraft receives the travel request between two aerodromes from an individual customer, the aircraft will determine the flight plan (e.g., the route selection of corridors, estimated travel time, and the aerodromes) which is subsequently submitted to the GBS via an air-to-ground link. Then, the GBS will evaluate the submitted plan against pre-determined constraints, such as the availability of corridors and aerodromes as well as possible conflicts with on-going operation of other aircraft. If the flight plan meets the constraints, then the GBS will approve the flight plan and share it with other GBSs via backhaul links. The aircraft will later operate in the en-route phase to pick up the customer, navigate along the selected corridors, and arrive at the destination aerodrome within the expected travel

This research was supported by the Office of Naval Research (ONR) under MURI Grant N00014-19-1-2621 and by the U.S. National Science Foundation under Grants CNS-1739642 and CNS-1941348, and by the Academy of Finland Project CARMA, by the Academy of Finland Project MISSION, by the Academy of Finland Project SMARTER, as well as by the INFOTECH Project NOOR.

T. Zeng and W. Saad are with Wireless@VT, Department of Electrical and Computer Engineering, Virginia Tech, Blacksburg, VA, 24061 USA (e-mail: tengchan@vt.edu; walids@vt.edu).

O. Semiari is with the Department of Electrical and Computer Engineering, University of Colorado, Colorado Springs, CO, 80918 USA (e-mail: osemiari@uccs.edu).

M. Bennis is with the Centre for Wireless Communications, University of Oulu, 90014 Oulu, Finland (e-mail:mehdi.bennis@oulu.fi).

time. Note that during the en-route phase, the aircraft must constantly communicate with the GBSs to inform any off-nominal events (e.g., deviation from the selected corridors) due to high winds, performance issues, and navigation degradation, and accordingly change its flight plan. Hence, reliable air-to-ground communications are of great importance for the effective and safe operation of UAM.

Since UAM operation is still at its infancy, most of the related research focus on market studies [3], public acceptance [4], and operational constraints [5]. There are few works studying the technical aspects of UAM operation. For example, a learning-based collision avoidance is proposed in [6] to allow multiple aircraft operating independently and keeping a safe distance among each other. In [7], the arrival process of aircraft is optimized to minimize the energy consumption while meeting the expected travel time. It is clear that, despite of the important role of communication networks in UAM operation, there is a lack of study to analyze the wireless connectivity of the aircraft when using UAM.

The *main contribution* of this paper is a novel, rigorous performance analysis of aircraft-to-GBS communication networks in UAM. In particular, we use stochastic geometry to model the spatial distribution of GBSs, corridors, and aircraft in UAM. First, we model the location of the GBSs as a two-dimensional Poisson point process (PPP). Then, due to the fact that corridors will be typically centralized around a number of popular destinations, we model the locations of these centralized points (CPs) as another two-dimensional PPP. Next, to capture the relative location between the CP and its corridors, we study two different models for the corridors' locations depending on whether the distance between the CP and the corridors follows a truncated Gaussian distribution or a uniform distribution. With this setup, we derive the Laplace transform of the interference suffered at a GBS and the communication distance distribution between the GBS and its associated aircraft, assuming that each aircraft communicates with its closest GBS. Using these results, we derive the signal-to-interference ratio (SIR)-based connectivity probability which provides us with a metric to characterize the performance of aircraft-to-GBS communication networks in UAM. *To the best of our knowledge, this is the first work that analyzes the connectivity performance of air-to-ground communication networks in a UAM scenario.* Simulation results are provided to validate our theoretical analysis for the connectivity study and show the performance for different parameters thus offering useful system design insight for deploying UAM.

The rest of the paper is organized as follows. Section II presents the system model for UAM. Section III provides the theoretical analysis for the aircraft's connectivity. Section IV presents simulation results, and conclusions are drawn in Section V.

II. System Model

Consider a group of aircraft operating in UAM, as shown in Fig. 1. During the flight, each aircraft will constantly communicate with a GBS to report its real-time location and trajectory as well as possible off-nominal events. Meanwhile, each aircraft will also share the flight plan with other aircraft via aircraft-to-aircraft communications so as to maintain a safe distance and avoid collisions during the operation.

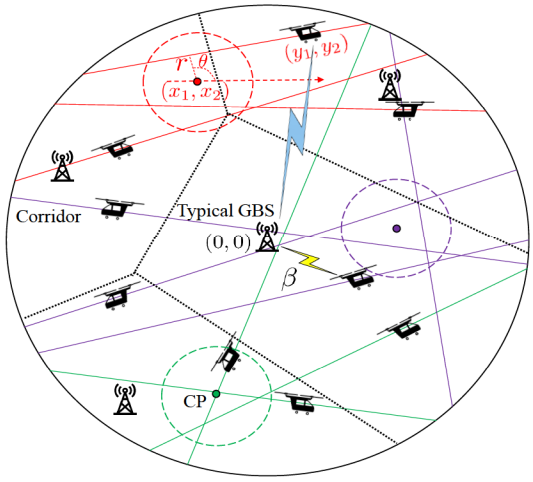

Fig. 2. The top view of how corridors, aircraft, centralized points, and ground base stations are distributed in UAM.

A. Spatial Models for UAM

In order to capture the wireless connectivity in UAM, we must study the spatial modeling of aircraft and GBSs. As shown in Fig. 2, we model the distribution of GBSs as a two-dimensional PPP Ξ with density λ_b. For the distribution of aircraft, we first model the spatial distribution of CPs and corridors. In particular, to capture the fact that the CPs can spread across the space, we model their distribution as a two-dimensional PPP Φ with density λ_c. Around CP $i \in \Phi$, we model the distribution of corridors as a Poisson line process (PLP) Ψ_i with density λ_l where all corridors share the same height h. Due to the fact that there will be a limited number of corridors around each CP, we assume that the maximum number of corridors for each CP is N. In this case, the number of corridors follows a Poisson distribution within the range of $[0, N]$.

Similar to [8], the relative location of a corridor around a CP is determined by two factors: the distance $r \in \mathbb{R}_+$ between the CP and the corridor and the angle $\theta \in [0, 2\pi)$ between the positive x-axis and the line passing through the CP and being perpendicular to the corridor, as shown in Fig. 2. However, instead of using a randomly distributed r in $\mathbb{R}_+$ which does not capture the realistic spatial location of centralized corridors, inspired by Poisson cluster process (PCP) [9], we model the distance r with the following two approaches. The first approach is aligned with the *Thomas cluster process* whereby we model the distance r as a truncated Gaussian distribution as follows:

$$f_R(r) = \sqrt{\frac{2}{\pi\sigma^2}} \exp\left(-\frac{r^2}{2\sigma^2}\right), r \in [0, \infty).$$

In the second approach, we model the distance r as a uniform random variable within $[0, \hat{r}]$ with $\hat{r}$ being the maximum distance from the CP, i.e.,

$$f_R(r) = \frac{1}{\hat{r}}, r \in [0, \hat{r}].$$

As such, we can guarantee that all corridors around the same CP will pass through a circular disc area with radius $\hat{r}$, similar to the definition of the *Matérn cluster process*. With these two approaches, we can characterize the fact that the corridors are closely distributed around their CPs instead of being spread over the whole space as defined in [8]. Next, on a randomly selected corridor $j \in \Psi_i$, we assume that the distribution of aircraft follows a one-dimensional PPP with density λ_a. If the probability that each aircraft functions as the transmitter is ρ, then the locations of the transmitting aircraft on corridor $j \in \Psi_i$ can be modeled as a one-dimensional PPP $\Omega_{i,j}$ with density $\lambda_t = \rho\lambda_a$ according to the PPP thinning theorem [8].

B. Aircraft-to-GBS Communication Model

Similar to many works using stochastic geometry in wireless communications [10]–[12], we assume that each aircraft will be served by the closest GBS. Due to the stationarity of the two-dimensional PPP, we arbitrarily select a GBS as the *typical GBS* and assume that it is located at the origin with zero height. Thus, we can calculate the received signal power at the typical GBS from its associated aircraft as

$$U = pg(h^2 + \beta^2)^{-\frac{\alpha}{2}}, \tag{1}$$

where p is the transmit power of aircraft, and β is the distance between the vertical projection of the associated GBS at the plane with height h and the associated aircraft. α is the path loss exponent, and g is the air-to-ground wireless channel gain. We model the communication channels as independent Nakagami channels with an integer m to characterize a wide range of fading environment.

While receiving the transmission from the associated aircraft, the typical GBS will experience interference from two sources. The first one relates to aircraft who communicate with other GBSs rather than the typical GBS. The second source is aircraft who share the flight plan to surrounding aircraft. Taking into account the distribution of the transmitter aircraft in UAM, we can calculate the interference at the typical GBS as follows

$$I = \sum_{i\in\Phi}\sum_{j\in\Psi_i}\sum_{k\in\Omega_{i,j}} g'(||\boldsymbol{x} + \boldsymbol{y}||^2 + h^2)^{-\frac{\alpha}{2}}, \tag{2}$$

where, as shown in Fig. 2, $\boldsymbol{x} = (x_1, x_2)$ is the location of CP $i \in \Phi$ relative to the vertical projection of the typical GBS at the plane of height h, and $\boldsymbol{y} = (y_1, y_2)$ denotes the relative location of an interfering aircraft compared to its CP. Given the received signal and interference in (1) and (2), respectively, the SIR at the typical GBS can be calculated as $V = \frac{U}{I}$. For tractability, we assume that the noise is negligible compared to the interference and the communication network is interference limited.

Although there are many works using stochastic geometry to model wireless networks, their existing approaches cannot be directly applied to the air-to-ground communication network in UAM. The reason is that, different from wireless networks that can be simply modeled by a single point process, the spatial distribution of UAM aircraft is characterized by a combination of PPP, PCP, and PLP. In the following section, we take into account this complex distribution and analyze the connectivity performance when the aircraft communicate with its associated GBSs in UAM.

III. Connectivity Performance Analysis for Aircraft-to-GBS Communications in UAM

In this section, we first characterize the distance distribution of the typical GBS and its associated aircraft. Then, we calculate the Laplace transform of the interference experienced by the typical GBS. Next, we derive the SIR-based connectivity probability for the aircraft when operating in the UAM corridors.

A. Distance Distribution between the Typical GBS and its Associated Aircraft

Since each aircraft communicates with its closest GBS, we can derive the statistical distribution of the distance β between the vertical projection of the typical GBS and its associated aircraft in the following lemma that follows from [12].

Lemma 1. For a group of GBSs whose distribution follows a two-dimensional PPP with density λ_b, the probability density function (PDF) of the distance β between the vertical projection of the typical GBS and its associated aircraft is

$$f_B(\beta) = 2\pi\lambda_b\beta\exp(-\lambda_b\pi\beta^2). \tag{3}$$

With Lemma 1, we can calculate the statistical distribution of the distance between the typical GBS and its associated aircraft at height h, and further use (1) to determine the received signal power at the typical GBS.

B. Laplace Transform of Interference at the Typical GBS

In order to capture the interference experienced by the typical GBS, we need to model the distance between the typical GBS and the interfering aircraft. To this end, we start with the relative location $\boldsymbol{y} = (y_1, y_2)$ of the interfering aircraft around its CP. As shown in Fig. 3, we list four possible relative locations between CP and corridors. Assume that the projected point of CP on the corridor is $\boldsymbol{z} = (z_1, z_2)$ and the distance between $\boldsymbol{z}$ and the aircraft is $t \in \mathbb{R}$. Hence, we can obtain the four alternatives for the location of aircraft on the corridor as

$$\begin{cases} (z_1 + t\cos(\frac{\pi}{2} - \theta), z_2 - t\sin(\frac{\pi}{2} - \theta)), & \text{if } \theta \in [0, \frac{\pi}{2}), \\ (z_1 + t\cos(\theta - \frac{\pi}{2}), z_2 + t\sin(\theta - \frac{\pi}{2})), & \text{if } \theta \in [\frac{\pi}{2}, \pi), \\ (z_1 - t\cos(\frac{3\pi}{2} - \theta), z_2 + t\sin(\frac{3\pi}{2} - \theta)), & \text{if } \theta \in [\pi, \frac{3\pi}{2}), \\ (z_1 - t\cos(\theta - \frac{3\pi}{2}), z_2 - t\sin(\theta - \frac{3\pi}{2})), & \text{if } \theta \in [\frac{3\pi}{2}, 2\pi). \end{cases}$$

Meanwhile, the location of CP can be calculated as

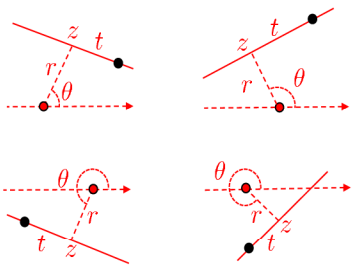

Fig. 3. Four possible relative locations between CP and corridors where the black solid point, red solid point, and solid line, respectively, show the aircraft, CP, and corridor.

$$\begin{cases} (z_1 - r\cos(\theta), z_2 - r\sin(\theta)), & \text{if } \theta \in [0, \frac{\pi}{2}), \\ (z_1 + r\sin(\theta - \frac{\pi}{2}), z_2 - r\cos(\theta - \frac{\pi}{2})), & \text{if } \theta \in [\frac{\pi}{2}, \pi), \\ (z_1 + r\sin(\frac{3\pi}{2} - \theta), z_2 + r\cos(\frac{3\pi}{2} - \theta)), & \text{if } \theta \in [\pi, \frac{3\pi}{2}), \\ (z_1 - r\cos(2\pi - \theta), z_2 + r\sin(2\pi - \theta)), & \text{if } \theta \in [\frac{3\pi}{2}, 2\pi). \end{cases}$$

Given the locations of the aircraft and CP for $\theta \in [0, 2\pi)$, we can identify the relative location $\boldsymbol{y} = (t\sin\theta + r\cos\theta, -t\cos\theta + r\sin\theta)$, $r \in \mathbb{R}_+, t \in \mathbb{R}$. Thereby, the distance between the vertical projection point of the typical GBS and the interfering aircraft is $f(x_1, x_2, t, r, \theta) = ||\boldsymbol{x} + \boldsymbol{y}|| = \sqrt{(x_1 + t\sin\theta + r\cos\theta)^2 + (x_2 - t\cos\theta + r\sin\theta)^2}$. Hence, we can determine the Laplace transform of the interference experienced by the typical GBS in the following lemma.

Lemma 2. When aircraft operating within UAM corridors are distributed according to the one-dimensional PPP, the Laplace transform of the interference experienced by the typical GBS is

$$\mathcal{L}(s) = e^{\left(-\lambda_c \int_{\mathbb{R}^+} \int_0^{2\pi} \left(1 - \sum_{n=0}^{N} (\mathcal{K}_2(l\cos\phi, l\sin\phi))^n \mathbb{P}(n|n<N)\right) l d\phi dl\right)}, \tag{4}$$

where $\mathbb{P}(n|n \leq N) = \frac{(\lambda_l - 1)^n e^{-(\lambda_l - 1)}}{n!\omega}$ with $\omega = \sum_{n=0}^{N} \frac{(\lambda_l - 1)^n e^{-(\lambda_l - 1)}}{n!}$, and $\mathcal{K}_2(l\cos\phi, l\sin\phi) =$

$$\int_{\mathbb{R}^+} \int_0^{2\pi} \mathcal{K}_1(l\cos\phi, l\sin\phi, r, \theta) f_R(r) f_\theta(\theta) d\theta dr,$$

with $\mathcal{K}_1(l\cos\phi, l\sin\phi, r, \theta) =$

$$e^{-\lambda_t \int_{\mathbb{R}} 1 - \left(\left(1 + \frac{s(f^2(l\cos\phi, l\sin\phi, t, r, \theta) + h^2)^{-\frac{\alpha}{2}}}{m}\right)^{-m}\right) dt}.$$

Proof: The Laplace transform of interference at the typical GBS can be derived as follows

$$\mathcal{L}(s) = \mathbb{E}[\exp(-s \sum_{i\in\Phi} \sum_{j\in\Psi_i} \sum_{k\in\Omega_{i,j}} g'(f^2(x_1, x_2, t, r, \theta) + h^2)^{-\frac{\alpha}{2}})]$$

$$= \mathbb{E}\left[\prod_{i\in\Phi} \prod_{j\in\Psi_i} \prod_{k\in\Omega_{i,j}} \mathbb{E}_{g'} \exp(-s g'(f^2(x_1, x_2, t, r, \theta) + h^2)^{-\frac{\alpha}{2}})\right]$$

$$\overset{(a)}{=} \mathbb{E}\left[\prod_{i\in\Phi} \prod_{j\in\Psi_i} \prod_{k\in\Omega_{i,j}} \left(1 + \frac{s(f^2(x_1, x_2, t, r, \theta) + h^2)^{-\frac{\alpha}{2}}}{m}\right)^{-m}\right]$$

$$= \mathbb{E}\left[\prod_{i\in\Phi} \prod_{j\in\Psi_i} \mathbb{E}_{\Omega_{i,j}} \prod_{k\in\Omega_{i,j}} \left(1 + \frac{s(f^2(x_1, x_2, t, r, \theta) + h^2)^{-\frac{\alpha}{2}}}{m}\right)^{-m}\right]$$

$$\overset{(b)}{=} \mathbb{E}\left[\prod_{i\in\Phi} \prod_{j\in\Psi_i} e^{-\lambda_t \int_{\mathbb{R}} 1 - \left(\left(1 + \frac{s(f^2(x_1, x_2, t, r, \theta) + h^2)^{-\frac{\alpha}{2}}}{m}\right)^{-m}\right) dt}\right]$$

$$= \mathbb{E}\left[\prod_{i\in\Phi} \mathbb{E}_{\Psi_i} \prod_{j\in\Psi_i} \underbrace{e^{-\lambda_t \int_{\mathbb{R}} 1 - \left(\left(1 + \frac{s(f^2(x_1, x_2, t, r, \theta) + h^2)^{-\frac{\alpha}{2}}}{m}\right)^{-m}\right) dt}}_{\mathcal{K}_1(x_1, x_2, r, \theta)}\right]$$

$$\overset{(c)}{=} \mathbb{E}_\Phi\left[\prod_{i\in\Phi} \sum_{n=0}^{N} \left(\underbrace{\int_{\mathbb{R}^+} \int_0^{2\pi} \mathcal{K}_1(x_1, x_2, r, \theta) f_R(r) f_\theta(\theta) d\theta dr}_{\mathcal{K}_2(x_1, x_2)}\right)^n \mathbb{P}(n|n \leq N)\right]$$

$$\overset{(d)}{=} \exp\left(-\lambda_c \int_{\mathbb{R}^2} \left(1 - \sum_{n=0}^{N} (\mathcal{K}_2(x_1, x_2))^n \mathbb{P}(n|n \leq N)\right) dx\right)$$

$$\overset{(e)}{=} e^{\left(-\lambda_c \int_{\mathbb{R}^+} \int_0^{2\pi} \left(1 - \sum_{n=0}^{N} \mathcal{K}_2(l\cos\phi, l\sin\phi)^n \mathbb{P}(n|n\leq N)\right) l d\phi dl\right)}, \tag{5}$$

where (a) follows the Gamma distribution of Nakagami fading channel gains, (b) and (d) are based on the probability generating functional (PGFL) of a PPP [8]. In (c), we use the fact that the number of corridors is Poisson distributed conditioned on total being less than N. The simplification in (e) is done by converting from Cartesian to polar coordinates with $x_1 = l\cos\phi$ and $x_2 = l\sin\phi$. ■

By choosing the proper function $f_R(r)$ in Lemma 2, we can calculate the Laplace transform of the interference when the distance between the corridor and its CP follows a truncated Gaussian distribution or a uniform distribution. Next, we use the Laplace transform of the interference obtained in Lemma 2 to determine the connectivity performance of air-to-ground communications in UAM.

C. Connectivity Probability

The connectivity probability is defined as the probability where the SIR received by the typical GBS exceeds a target threshold γ required for a successful communication. Based on the Laplace transform of the interference obtained in Lemma 2, we can derive the mathematical expression for the connectivity probability in the following theorem.

Theorem 1. When an arbitrarily selected aircraft communicates with its associated GBS in UAM, the connectivity probability can be calculated as

Table. I. Simulation parameters.

Parameters	Values
Height h	500 feet (152.4 m) [2]
CP density λ_c	0.001 $(\text{km}^2)^{-1}$
GBS density λ_b	1 $(\text{km}^2)^{-1}$
Corridor density λ_l	5 corridor/km^2
Aircraft density λ_a	1 aircraft/km
Maximum number of corridors N	10
Transmit power T_r	40 dBm
SIR threshold γ	0 dB
Path loss exponent α	4
Nakagami fading parameter m	1
Probability that a random aircraft is a transmitter ρ	0.5
Variance of truncated Gaussian distribution σ^2	1
Distance limitation for the uniform distribution $\hat{r}$	2 km

$$\mathbb{P}_{\text{conn}} = \int_{\mathbb{R}^+} \sum_{\hat{m}=1}^{m} (-1)^{\hat{m}+1} \binom{m}{\hat{m}} \mathcal{L}(\hat{m}\eta\gamma(h^2+\beta^2)^{\frac{\alpha}{2}}) f_B(\beta) d\beta. \tag{6}$$

where $\eta = m(m!)^{-1/m}$.

Proof: The connectivity probability can be calculated as follows

$$\begin{aligned}
\mathbb{P}_{\text{conn}} &= \mathbb{E}\left[\mathbb{P}(V \geq \gamma|\beta)\right] = \mathbb{E}\left[\mathbb{P}\left(\frac{g(h^2+\beta^2)^{-\frac{\alpha}{2}}}{I} \geq \gamma|\beta\right)\right] \\
&= \mathbb{E}\left[\mathbb{P}\left(g \geq \frac{\gamma I}{(h^2+\beta^2)^{-\frac{\alpha}{2}}}|\beta\right)\right] \\
&\overset{(a)}{\approx} 1 - \mathbb{E}\left[\left(1 - \exp\left(\frac{-\eta\gamma I}{(h^2+\beta^2)^{-\frac{\alpha}{2}}}\right)\right)^m |\beta\right] \\
&\overset{(b)}{=} \sum_{\hat{m}=1}^{m} (-1)^{\hat{m}+1} \binom{m}{\hat{m}} \mathbb{E}\left[\exp\left(\frac{-\hat{m}\eta\gamma I}{(h^2+\beta^2)^{-\frac{\alpha}{2}}}\right)|\beta\right] \\
&\overset{(c)}{=} \int_{\mathbb{R}^+} \sum_{\hat{m}=1}^{m} (-1)^{\hat{m}+1} \binom{m}{\hat{m}} \mathcal{L}(\hat{m}\eta\gamma(h^2+\beta^2)^{\frac{\alpha}{2}}) f_B(\beta) d\beta,
\end{aligned} \tag{7}$$

where (a) is based on the approximated tail probability of a Gamma function [13], (b) follows the Binomial theorem and the assumption that m is an integer, and (c) follows the definition of Laplace transform of interference and the fact that the distance between the aircraft and GBS is a random variable. ■

With Theorem 1, we can theoretically analyze the connectivity performance of aircraft-to-GBS communication networks in UAM. The results in Theorem 1 also pave the way for optimizing the UAM design to achieve a reliable wireless connectivity and ensure an efficient and safe UAM operation.

IV. Simulation Results

We use MATLAB for our simulations. In particular, we consider a circular area with a radius of 20 km and the values of the different parameters are summarized in Table I. We first validate the theoretical analysis in Theorem 1 for distance r that follows the truncated Gaussian distribution and uniform distribution. Then, we study how the densities of GBSs, CPs, corridors, and aircraft affect the wireless connectivity performance and provide insights into the system design guidelines for UAM.

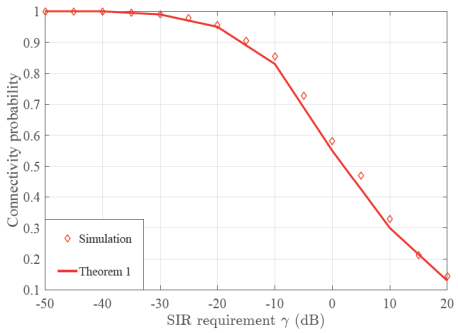

(a) Truncated Gaussian distribution for the distance r between the CP and corridors.

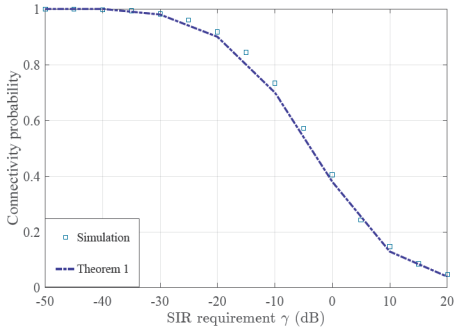

(b) Uniform distribution for the distance r between the CP and corridors.

Fig. 4. Connectivity probability of the UAM wireless network versus the SIR threshold.

A. Validation of Theoretical Results

Fig. 4 shows the connectivity probability of the air-to-ground communication network versus the SIR threshold γ when the distance r follows a truncated Gaussian distribution and a uniform distribution. As observed from Fig. 4, the simulation results for both distributions match the analytical results with a small deviation. The small deviation stems from the use of the approximated tail probability of Gamma function in Theorem 1. Fig. 4 also shows that, when the SIR threshold γ increases, the connectivity performance of the UAM's wireless network will degrade. This is because, with a higher target SIR threshold, fewer air-to-ground communication links will meet the requirement for a successful transmission.

B. Connectivity Performance of UAM under Different Parameter Settings

Fig. 5 shows the connectivity probability of the UAM wireless network versus the corridor density λ_l under different values for the cluster density λ_c when the distance follows a truncated Gaussian distribution. From Fig. 5, we observe that the connectivity probability decreases when the corridor

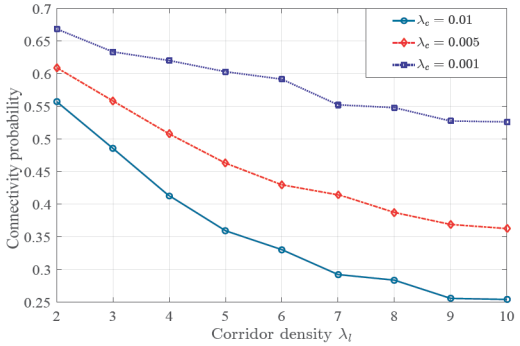

Fig. 5. Connectivity probability of the UAM wireless network versus the corridor density under different cluster densities.

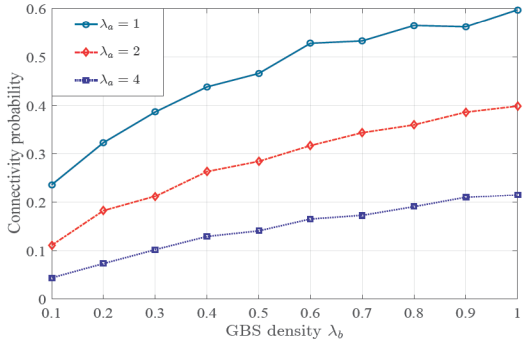

Fig. 6. Connectivity probability of the UAM wireless network versus the GBS density under different aircraft densities.

density λ_l increases. This is due to the fact that, with more corridors distributed around the CPs, the number of interfering aircraft will also increase, leading to a higher interference at the typical GBS and a degradation of the wireless connectivity performance. Moreover, Fig. 5 shows that a higher density of CPs will also degrade the UAM wireless connectivity performance. This is because, a higher density of CPs will lead to more corridors and more interfering aircraft.

Fig. 6 shows the connectivity probability of the UAM wireless network versus the GBS density λ_b under different aircraft density λ_a on each corridor and for the case when the distance follows a truncated Gaussian distribution. As shown in Fig. 6, the connectivity probability increases when the GBS density λ_b increases. This is because, with more GBSs, the communication distance between a given GBS and its associated aircraft flying in UAM will be reduced, leading to a higher received signal power and SIR. Moreover, Fig. 6 shows that the presence of more aircraft on corridors will negatively impact the connectivity probability performance. This can be explained by noting that a higher λ_a will increase the number of interfering aircraft when the probability that each aircraft functions as the transmitter is fixed. Note that the simulation results of the uniformly distributed distance r are similar to the counterparts for the truncated Gaussian distributed distance, and they are omitted due to space limitations.

Based on the simulation results in Figs. 5 and 6, when the densities of aircraft, corridors, and CPs increase, the UAM wireless connectivity performance will degrade. To avoid this performance degradation, one can deploy more GBSs at the expense of site acquisition constraints and costs, particularly in urban environments. Therefore, realizing efficient UAM systems depends on a careful selection of design parameters to improve the wireless connectivity performance while reducing the overall deployment cost.

V. Conclusions

In this paper, we have used stochastic geometry to analyze the performance of wireless communications in UAM. In particular, we have leveraged PCP and PLP to capture the relative location of corridors around their CPs where the relative distance between them is modeled by two distributions: truncated Gaussian distribution and uniform distribution. Moreover, we have characterized the distribution of aircraft on each corridor by using a one-dimensional PPP. In addition, we have modeled the distribution of GBSs according to the two-dimensional PPP. Using this system setup, we have derived new theoretical results for the SIR-based connectivity probability when the aircraft communicates to its closest GBS. Simulation results corroborate our connectivity analysis for UAM and show how different system settings affect the overall connectivity performance.

References

[1] United Nations, Department of Economic and Social Affairs, "World urbanization prospects the 2018 revision," 2018.

[2] Federal Aviation Administration, "Concept of operations v1.0, foundational priciples, roles and responsibilities, scenarios and operational threads, urban air mobility (UAM)," Jun. 2020.

[3] Booz Allen Hamilton, "Urban air mobility (UAM) market study," 2018.

[4] C. Al Haddad, E. Chaniotakis, A. Straubinger, K. Plötner, and C. Antoniou, "Factors affecting the adoption and use of urban air mobility," *Transportation Research Part A: Policy and Practice*, vol. 132, pp. 696–712, Feb. 2020.

[5] P. D. Vascik, J. Cho, V. Bulusu, and V. Polishchuk, "Geometric approach towards airspace assessment for emerging operations," *Journal of Air Transportation*, vol. 28, no. 3, pp. 124–133, May 2020.

[6] A. Rodionova, Y. V. Pant, K. Jang, H. Abbas, and R. Mangharam, "Learning-to-fly: Learning-based collision avoidance for scalable urban air mobility," in *Proc. of IEEE International Conference on Intelligent Transportation Systems (ITSC)*, Rhodes, Greece, Sept. 2020.

[7] P. Pradeep and P. Wei, "Energy-efficient arrival with RTA constraint for multirotor evtol in urban air mobility," *Journal of Aerospace Information Systems*, vol. 16, no. 7, pp. 263–277, Jul. 2019.

[8] S. N. Chiu, D. Stoyan, W. S. Kendall, and J. Mecke, *Stochastic geometry and its applications*. John Wiley & Sons, 2013.

[9] M. Haenggi, *Stochastic geometry for wireless networks*. Cambridge University Press, 2012.

[10] V. V. Chetlur and H. S. Dhillon, "Coverage analysis of a vehicular network modeled as cox process driven by poisson line process," *IEEE Transactions on Wireless Communications*, vol. 17, no. 7, pp. 4401–4416, Jul. 2018.

[11] C. Choi and F. Baccelli, "Poisson cox point processes for vehicular networks," *IEEE Transactions on Vehicular Technology*, vol. 67, no. 10, pp. 10 160–10 165, Oct. 2018.

[12] J. G. Andrews, A. K. Gupta, and H. S. Dhillon, "A primer on cellular network analysis using stochastic geometry," *arXiv preprint arXiv:1604.03183*, 2016.

[13] T. Bai and R. W. Heath, "Coverage and rate analysis for millimeter-wave cellular networks," *IEEE Transactions on Wireless Communications*, vol. 14, no. 2, pp. 1100–1114, Feb. 2015.